Journal of Environmental Radioactivity 283 (2025) 107623

Contents lists available at ScienceDirect

Journal of Environmental Radioactivity

journal homepage: www.elsevier.com/locate/jenvrad

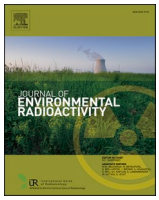

Analysis of ^{127}Xe tracer measurements using a net counts method

M.A. Goodwin [a,*], D.L. Chester [a], G. Galvin [a], P.W. Eslinger [b], M. Foxe [b], J. Ely [b], R. Turley [c], PE-1 Experiment Team [1]

[a] AWE Aldermaston, Reading, RG7 4PR, UK
[b] Pacific Northwest National Laboratory (PNNL), 902 Battelle Blvd., Richland, 99354, WA, USA
[c] Nevada National Security Sites (NNSS), Mercury, Nevada, USA

ARTICLE INFO

Keywords:
CTBT
International monitoring system
Radioxenon
Nuclear explosion monitoring
Physical experiment 1
Xe-127

ABSTRACT

A suite of measurement systems were deployed as part of the Physical Experiment 1 series of experiments, which involved detonating chemical explosives along with radionuclide tracers in an underground cavity, at the Nevada National Security Site (NNSS) in the United States. One of the radionuclide tracers, ^{127}Xe was released from the containment following the explosion and detected on a SAUNA Q_B sampler situated approximately 3.5 km away. The system uses a beta-gamma coincidence detector system to measure fission product radioisotopes of xenon relevant to nuclear explosion monitoring. In this work we use the coincidence measurement data to analyse and interpret the results from the SAUNA Q_B system, to calculate the measured ^{127}Xe activity concentration(s).

1. Introduction

1.1. Overview

This work involves the activity quantification of ^{127}Xe in environmental xenon samples collected using an automatic radioxenon sampler/analyser system at the Nevada National Security Site (NNSS, US). The detector system had previously been calibrated for fission product radioxenon isotopes used for routine nuclear explosion monitoring, and so work was required to calibrate the system for ^{127}Xe, which produces a complex β-γ coincidence measurement spectra. This work summarises the coincidence measurement signatures of ^{127}Xe for a plastic scintillator and NaI(Tl) based detector system, using both measurement and modelling approaches to determine the detectability of each signal, in order to quantify ^{127}Xe from data collected during a field experiment.

1.2. Background

Radionuclides are monitored routinely in the atmosphere as part of international efforts to verify the Comprehensive Nuclear-Test-Ban Treaty (CTBT) (United Nations, 1996) but whilst there are many examples of anthropogenic radionuclides detected on radionuclide monitoring networks, there are few examples of detection of radionuclides from an underground nuclear test (Bowyer, 2021). The International Monitoring System (IMS) was designed to detect radionuclides from a nuclear explosion; it is significantly more challenging to detect the possible radionuclide emissions from an underground nuclear test (Goodwin et al., 2024a).

1.3. Physical Experiment 1

Monitoring radionuclides possibly related to underground nuclear explosions can require assumptions about the ground truth location, containment, source term and source composition. As part of a research and development programme to improve understanding of the signals associated with a low-yield underground nuclear explosion, a variety of radionuclide monitoring equipment has been deployed as part of Physical Experiment 1 (PE1) – a series of chemical explosive shots at the NNSS in the US. A full overview of the PE-1 experiments and particularly Shot A, can be found in an online report (Myers et al., 2024).

One of the radioactive tracers used in the experiment was ^{127}Xe, a tracer for the isotopes of radioxenon expected from a nuclear explosion (primarily the fission product radioisotopes – ^{133}Xe, ^{135}Xe, ^{131m}Xe, ^{133m}Xe). Around 1 Ci (3.7×10^{10} Bq) of ^{127}Xe ($t_{1/2} = 36.3$ d) was added to the explosion cavity and subsequently released during the explosion.

* Corresponding author.
E-mail address: matthew.goodwin@awe.co.uk (M.A. Goodwin).

[1] A multi-Physics Experiment for Low-Yield Nuclear Explosion Monitoring, LLNL-TR-864107, 2024, Lawrence Livermore National Laboratory, Livermore, California, United States.

https://doi.org/10.1016/j.jenvrad.2025.107623
Received 4 October 2024; Received in revised form 15 January 2025; Accepted 20 January 2025
Available online 4 February 2025

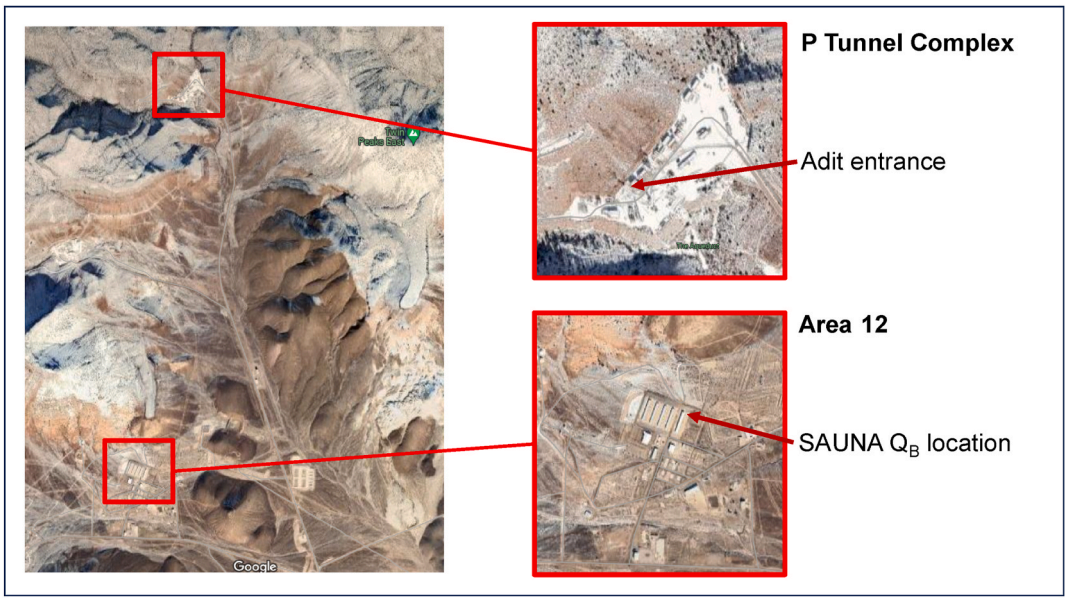

Fig. 1. Satellite images showing the location of the explosion and the location of the SAUNA Q_B sensor. Credit: Google.

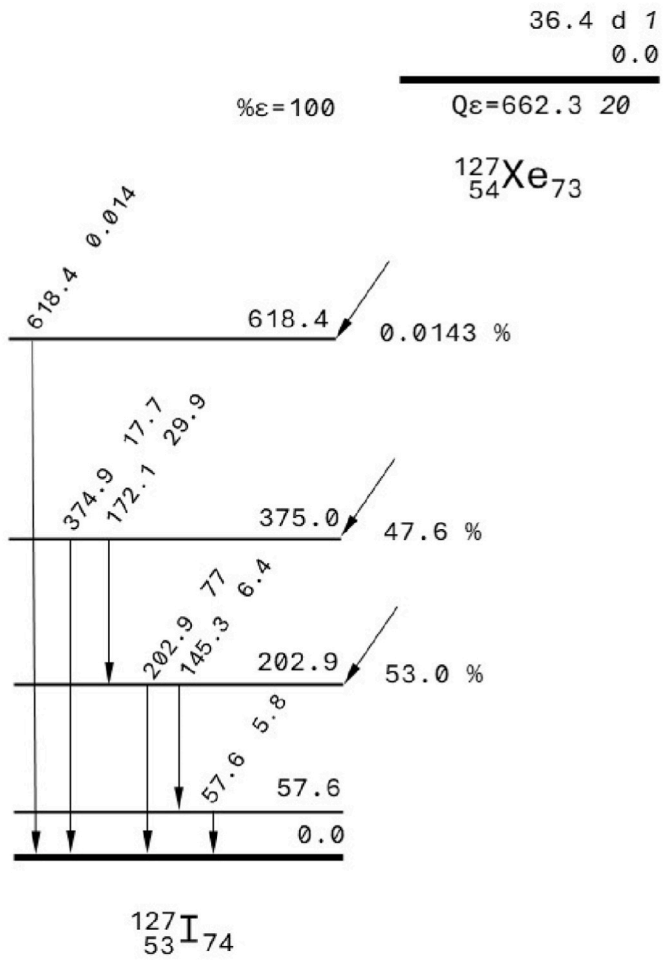

Fig. 2. Simplified nuclear decay scheme for the electron capture (EC) decay of ^{127}Xe to energy states of ^{127}I, showing main de-excitations. Energy units are keV and intensities are shown as percentages. This figure has been reproduced using data from Nuclear Data Sheets (Hashizume, 2011).

Numerous systems were deployed to monitor for the release of gases from the explosion cavity, including a SAUNA Q_B system which has previously been used in array-like configurations across Europe (Ringbom et al., 2023; Goodwin et al., 2024b). Systems similar to the SAUNA Q_B are routinely used on global monitoring networks such as the IMS. This experiment involves the fielding of a Q_B at a much closer range.

In the hours following the explosion, the ^{127}Xe tracer was detected in various boreholes and in the tunnel environment. There were then 3 venting events. The first was where the ventilation system was activated to evacuate HE byproduct gases that had entered the tunnel environment. The second was a few days later to allow workers back into the tunnel. The third was around one month later to ventilate a different part of the tunnel complex. This work provides an overview of the analysis of a measurement dataset collected in the field during the experiment, in order to determine whether ^{127}Xe was detected on the most remote radionuclide measurement system fielded for this experiment (3.5 km) – the SAUNA Q_B. This dataset covers the entire period around the explosion, with measurements collected before, during and after the releases.

1.4. SAUNA Q_B

The SAUNA Q_B samples and purifies xenon, quantifies the xenon gas volume, then measures the radioxenon content using a beta-gamma coincidence spectrometry system consisting of a NaI(Tl) photon detector and plastic scintillator electron detector or "beta cell". The system has previously been involved in monitoring radioxenon emissions from a nuclear power station in the UK (Goodwin et al., 2024b).

For the first part of the PE1 experiment, the SAUNA Q_B was installed at area 12 in the Nevada National Security Site (NNSS), approximately 3.5 km from the entrance to P Tunnel (see Fig. 1).

2. Method

2.1. Deriving a calibration

^{127}Xe decays via electron capture decay to excited levels of ^{127}I (see Fig. 2), where a series of transitions (some strongly converted) can produce electron-photon coincidences detectable using a SAUNA-type detector system (Klingberg et al., 2015). Fig. 3 shows a measurement

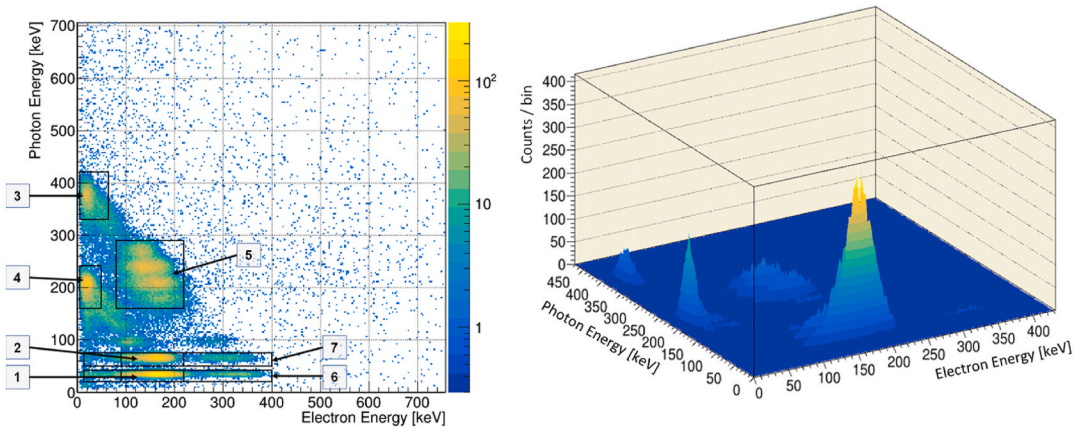

Fig. 3. ^{127}Xe measurement on a SAUNA-style beta-gamma coincidence detector. Left: showing the regions of interest used for the analysis of ^{127}Xe in these samples (from Robinson et al., 2024) and right: showing a 3D representation of the coincidence matrix from this measurement, giving a better visualisation of the relative signal resolution and magnitude.

Table 1
ROI definitions and a summary of some of the main signatures. $\gamma_0 = 57$ keV, $\gamma_1 = 145$ keV, $\gamma_2 = 172$ keV, $\gamma_3 = 202$ keV, $\gamma_4 = 375$ keV. X(K) refers to a K-shell X-ray. * denotes that the X-ray can be produced from either the EC decay or from internal conversion during a coincident cascading de-excitation. Coincidences can occur where a γ-ray is missed/not-detected but then the next de-excitation is detected.

ROI	E_e low [keV]	E_e high [keV]	E_γ low [keV]	E_γ high [keV]	Contributing signatures *[Electron signature in italics]*
1	90	220	20	42	*K(CE)*γ_1 + X(K)* *K(CE)*γ_2 + X(K)* *K(CE)*γ_3 + X(K)* Plus the above with Auger (K) electron
2	90	220	50	75	*K(CE)*γ_1+ γ_0 *K(CE)*γ_2+ γ_0 ROI 1 + X-ray sum
3	5	65	330	420	*K-Auger* + γ_4 *K-Auger* + γ_2+ γ_3
4	5	50	160	242	*K-Auger* + γ_3
5	80	220	160	275	*K(CE)*γ_2 + γ_3 *K(CE)*γ_3 + γ_2 *K(CE)*γ_2 + γ_3 + X(K)* *K(CE)*γ_3 + γ_2 + X(K)* *K(CE)*γ_2 + γ_3 + 2X(K)* *K(CE)*γ_3 + γ_2 + 2X(K)* *K(CE)*γ_3 + *K-Auger* + γ_2 + X(K)*
6	14	400	20	42	*Incl. ROI 1* *K(CE)*γ_4 + X(K) *K(CE)*γ_4 + *K-Auger* + X(K)
7	14	400	50	75	*Incl. ROI 2* *K(CE)*γ_4 + $X(K)_{x2}$

of a radiopure ^{127}Xe sample on a SAUNA-II detector system (Ringbom et al., 2003). Measurements conducted at the UK CTBT Radionuclide laboratory at AWE (Aldermaston, UK) were used to determine the regions of interest (ROIs) and associated calibration factors. The measurements were compared to high resolution gamma (γ)-ray spectrometry measurements traceable to a primary standard (Robinson et al., 2024). The ROIs identified and used for quantification in that work are annotated on Fig. 3 and summarised in Table 1.

Measurements are useful to understand the detector response, but due to the limited energy resolution of the SAUNA-type detectors, do not provide full information on the nuclear decay modes, but rather a combination of the coincidence signatures from nuclear decay as well as various summing signatures. To provide more information, a GEANT4 model of a SAUNA-II detector system was developed (see Eslinger et al., 2024) and used to derive the probability of an interaction in each ROI.

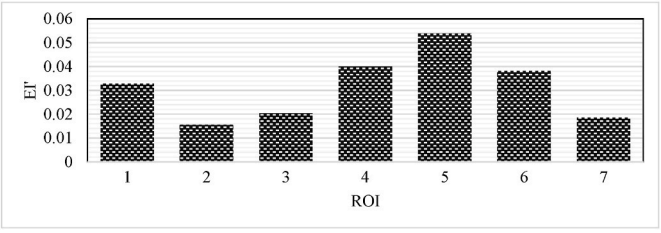

Fig. 4. Calculated Efficiency-Intensity products for a SAUNA Q_B detector system, using the ROIs defined in Fig. 3.

Table 2
ROIs for ^{127}Xe analysis of the beta-gamma coincidence spectra, with simulation-derived (GEANT4) efficiency-intensity products (EI), correction factor (F) and final product (EI').

ROI	EI	F	EI'
1	0.0340	0.964	0.0328
2	0.0158	0.986	0.0156
3	0.0204	1	0.0204
4	0.0399	1	0.0399
5	0.0539	1	0.0539
6	0.0396	0.964	0.0382
7	0.0189	0.986	0.0186

The dimensions of the SAUNA Q_B beta cell are slightly larger (~18 cm^3) than that of a SAUNA-II system (~6 cm^3) and as such, there are differences in the photon detection efficiencies between the two detectors. The beta efficiencies are effectively 100 % for both types. A correction factor, equivalent to the ratio of the energy-dependent photon detector efficiency, is applied to ensure the calibration is relevant to a SAUNA Q_B detector system. Equation (1) shows the correction applied to the model using the ratio of gamma efficiencies in the two systems, where $\varepsilon_{\beta\gamma}(ROI_i)$ is the beta-gamma efficiency ROI i and $\varepsilon_\gamma(ROI_i)$ is the corresponding gamma efficiency. For all regions considered here, the maximum correction applied was 3.6 % relative (ROI 1).

$$\varepsilon_{\beta\gamma}(ROI_i)' = \varepsilon_{\beta\gamma}(ROI_i) \times \frac{\varepsilon_\gamma(ROI_i)(Q_B)}{\varepsilon_\gamma(ROI_i)(SAUNAII)}$$

The final values are shown in Fig. 4 and given in Table 2. A useful discussion of the electron-photon coincidence signatures from the decay of ^{127}Xe is available in the literature (Cagniant et al., 2014). There are no correction factors for regions with photon energies greater than 200 keV, as the calculated difference in efficiency is negligible.

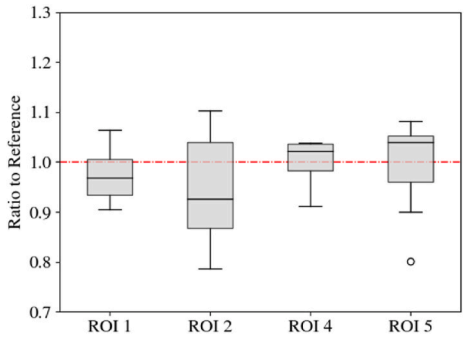

Fig. 5. Boxplots showing the calibration measurement results compared to the reference value (independently based on standard γ-ray spectrometry).

If measurements of samples containing ^{127}Xe were processed using a standard method, there would likely lead to false positive detections of ^{131m}Xe, ^{133m}Xe and ^{133}Xe and possibly ^{135}Xe, since the decay of ^{127}Xe results in coincidence signatures that would contribute counts to the ROIs used to derive the concentration of the other isotopes of radioxenon (Eslinger et al., 2022).

Previous work has shown the variability of self-attenuation effects in different ROIs (Robinson et al., 2024). In this work the xenon volume is broadly the same throughout the sampled period, so no further correction has been made for the xenon volume in the detector cell since the simulation accounted for around 1 cm^3 of xenon gas in the detector cell.

Of the ROIs listed above, validation measurements of known concentrations of ^{127}Xe in a SAUNA-II detector cell and calculation of the activity using the efficiency-intensity (EI) products shown in Table 2 have shown that activity concentrations calculated from ROIs 1, 2, 4 and 5 demonstrate good agreement with the reference value. ROI 3 was consistently low and showed a strong xenon volume dependency, and ROI 7 was consistently high, but showed minor xenon volume dependency. Whilst the results are shown for all ROIs, for the purposes of calculating the final activity concentration in this work, ROIs 1, 2, 4 and 5 will be used. ROI 6 was also in good agreement; however, this was removed to limit the regions to four that do not overlap. The overall comparison between results from the β-γ coincidence spectrometry method and the high resolution γ-ray spectrometry method agree to within a few percent. Fig. 5 shows results of the laboratory calibration measurements for the ROIs selected for quantification in this work.

2.2. Environmental data

Once installed and operational, the SAUNA Q_B system compresses and processes air over a period of 12 h. The xenon gas is then processed and quantified using a gas chromatograph. The system sampled and processed around 1.3 cm^3 (STP) of xenon in each 12-h cycle. The amount of xenon in each sample is an indicator of the system's state of health, although is sensitive to a number of other factors, including the environmental temperature (lower temperatures result in more xenon sampled). The equivalent air volume is determined from the known fraction of xenon in air (0.087 cm^3 per 1 m^3 air) (Glueckauf, 1951). The system was operated for the experiment between mid-September to late November. Other data from this system is available to support understanding any background signatures (Miley and Eslinger, 2022), however only the data around the experiment time is used here.

The measurement data was analysed for the whole period using the standard net counts correction (NCC) method and no detections of ^{133}Xe, ^{131m}Xe, ^{133m}Xe or ^{135}Xe were observed, inside or outside of the period of interest. The analysis discussed here is conducted on the assumption that there is no fission product radioxenon gas present in any of the samples. Therefore no corrections have been applied to correct for the interferences of other isotopes; ^{127}Xe is the only isotope considered.

Table 3
Background count rates for each ROI.

ROI	Count rate (Counts per 1000 s)	σ (±)	σ (%)
1	0.95	0.25	25.97
2	0.99	0.29	28.95
3	3.20	0.47	14.80
4	4.59	0.44	9.67
5	7.92	0.54	6.85
6	4.21	0.60	14.16
7	5.52	0.59	10.70

2.3. System performance

During the period of operations in the NNSS, the SAUNA Q_B performed well. Data from the system was remotely checked each day to ensure there were no issues. At the end of October 2023, the collection efficiency dropped and the amount of xenon in each sample reduced by approximately 30% to around 0.9 cm^3 (see Fig. 6). This negatively impacts the detection limits, but fortunately the main most important period of data was before this occurred. The reason for this is currently unknown, but most likely related to loss of pump efficiency, possibly due to a small pressure leak. The system will be fully serviced before more measurements are conducted.

2.4. Detector backgrounds and activity calculation

The background signal and variation from measurement to measurement was quantified and used to derive a standard background for all ROIs. The background measurements are completed in 5-h acquisitions, separated by quality control measurements to correct for any energy drift in the detectors. The total summed background acquisition length was 4 days (96 h) and the measured count rates are given in Table 3.

These background count rates were subtracted directly from the measured count rate to calculate the net count rate. The background count rate is also an important part of determining the detection limit for each signature.

The activity is calculated using Equation (2).

$$A = \frac{C_{net} \bullet K}{\varepsilon I' \bullet t_{live}}$$

Where C_{net} is the net counts in a region, K is the multiplicative decay correction factor for the periods of measurement, processing and sampling, εI is the electron-photon coincidence efficiency ($\varepsilon_{\beta\gamma}$) and intensity of the decay (I) product (including any summing-in/out or Compton effects); t_{live} is the acquisition live time (s). The full decay correction factor is given in Equation (3) and accounts for the period of measurement (first set of parentheses), period of sampling (second set of parenthesis) and intermediary period of processing (final term) and uses the decay constant (λ) for ^{127}Xe (2.207E-07 s^{-1}), measurement real time (t_{real}), sampling or collection time (t_s) and processing time (t_w) where all time values are given in seconds. The value of K is a constant (1.00665) for this single-nuclide, single-system case, since the values of t_s, t_w and t_{real} are constant for each sample.

$$K = \left(\frac{\lambda \bullet t_{real}}{1 - e^{-\lambda \bullet t_{real}}}\right)\left(\frac{\lambda \bullet t_s}{1 - e^{-\lambda \bullet t_s}}\right)e^{-\lambda \bullet t_w}$$

The 95% confidence detection limit (known as the minimum detectable concentration or MDC) and 68% confidence limit (known as the critical limit, or L_c) are used as thresholds to determine whether there is any ^{127}Xe detected. These are defined in other works such as Goodwin et al., 2020.

Atmospheric radioxenon measurements are usually reported in units of mBq per m^3 of air, which is calculated using Equation (4), where the effective volume of sampled air is calculated from the measured xenon volume and known fraction in air (0.087 cm^3 xenon per m^3 air). The

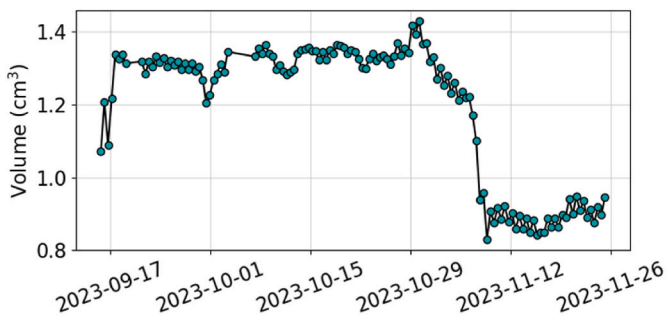

Fig. 6. Measured sampled xenon volume throughout the experiment. Uncertainties bars are excluded for clarity but the volume quantification uncertainty is around 5 % at k = 1 (one standard deviation).

results from this analysis campaign are reported as mBq/m^3.

$$A_c = \frac{A}{V_{Air}}$$

3. Results

3.1. Spectral data

Measurement spectra are shown in Figs. 7-9. The coincidence energy spectra are shown in Fig. 7 for four consecutive samples. The second measurement shows the highest count rates in the ^{127}Xe ROIs. Further analysis (results detailed in Section 3.2) shows the samples with collection start dates of 2023–10-20 04:38 UTC and 2023-10-20 16:38 UTC contain detectable levels of ^{127}Xe. Fig. 8 shows the beta-gated gamma spectra for the consecutive samples beginning with the sample prior to the first detection. There is a visible signal in the (red) shaded region which corresponds to increased count rates in the region with photon energy around 200 keV and electron energy around 100–200 keV. Fig. 9 shows (X-ray and gamma-gated) electron spectra from the sample with the highest activity detection, clearly showing the coincidence electrons in the (red) shaded regions.

3.2. Activity results

The ^{127}Xe activity concentration results throughout the period of interest are shown in Fig. 10, where there are a number of features to explain. The first is a short outage around the end of September. This was due to a power loss and the system was restarted including a regeneration of the sampling and processing ovens. The second key feature is the coinciding increase in ROI activity concentrations around 20th October. Finally, the increase in detection limits (MDCs) across all ROIs from around 9th November onwards, which is due to deteriorated sampling performance resulting in lower xenon volume in the detector cell, as discussed in Section 2.3.

The data shown in Fig. 11 represent the mean results from the analysis of multiple ROIs and the final results for the samples containing

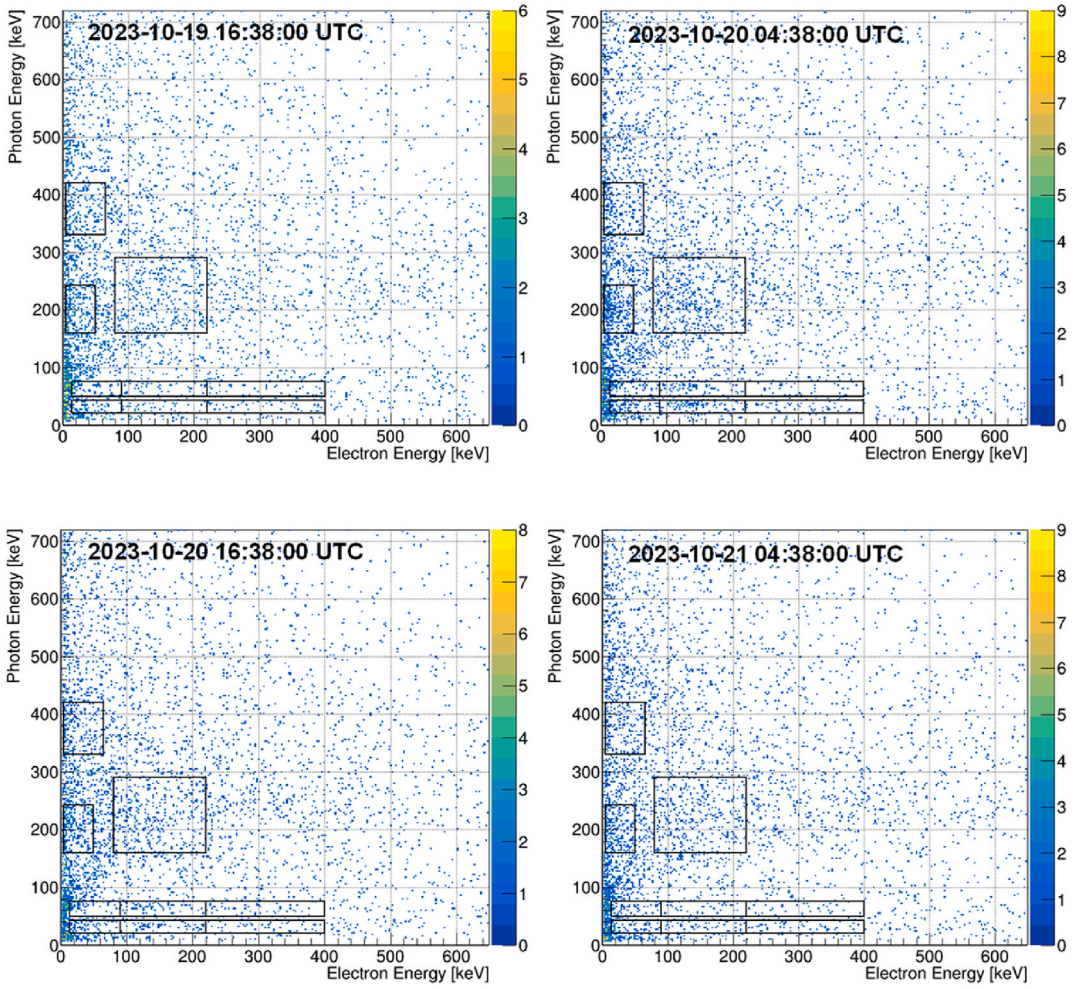

Fig. 7. Top-left to bottom-right, showing four consecutive sample measurements, where the middle two show increased count-rates in the ^{127}Xe regions of interest. The datetime shown corresponds to collection start.

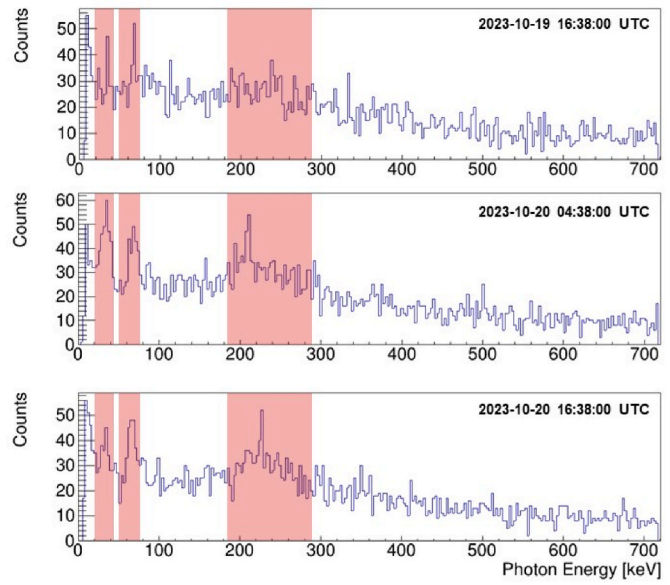

Fig. 8. Beta-gated gamma spectra (total coincidence) for (top to bottom) consecutive samples. The highlighted regions show ROI 1, 2 and 5 (which is inclusive of ROI 4). The bottom two samples contain clear spikes within the region and correspond with detections of ^{127}Xe.

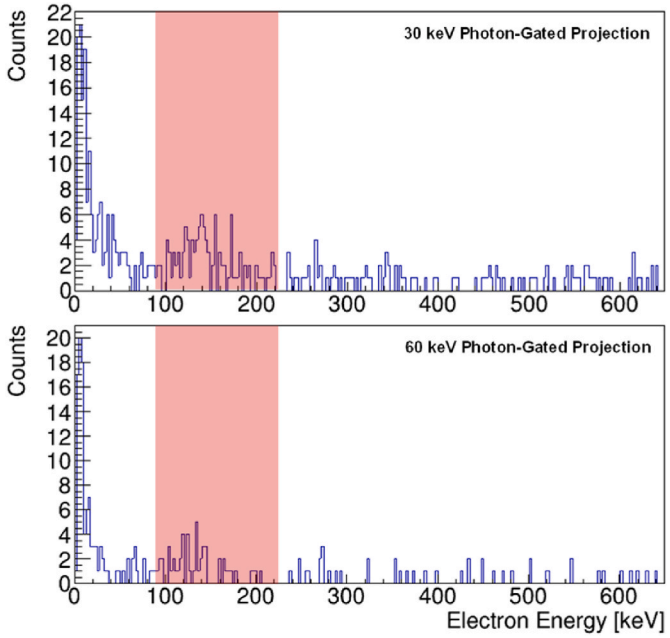

Fig. 9. Photon-gated projected electron coincidence spectra from the sample with collection start 2022-10-20 04:38:00 UTC. The top spectrum is from the 30 keV photon-gated projection, and the lower spectrum is from the 60 keV photon-gated projection. The red shaded regions correspond to the main regions of interest in the low-photon-energy part of the coincidence spectrum. The coincident electron peaks are visible at ~120–150 keV. (For interpretation of the references to colour in this figure legend, the reader is referred to the Web version of this article.)

detectable activities of ^{127}Xe are given in Table 4. Recent work by Eslinger et al., 2024 has analysed the same data using a new method known as Xcounts, which considers multiple ROIs at once.

4. Discussion

The analysis results presented here show two key detections of ^{127}Xe on the SAUNA Q_B system in the days following the explosion, and the hours following the initial activation of the ventilation system in the tunnel. An in-depth analysis of the spectra from the sample measurements around the time of the explosion show clear signatures which match with the expected ROIs from the simulations and previous work. The detection limits were calculated using standard Currie approach which were sufficient to determine which samples contained quantifiable ^{127}Xe activities. Taking ROI 1 alone yields lower detection limits than when averaging with less sensitive regions of the coincidence spectrum, however it is helpful to see that there are detectable signals in all identified regions of the spectrum, especially when the possibility of interference from other isotopes of radioxenon in the environment may require extra calculations.

Further to the confidence based on the validation of the analytical method, added confidence is derived from the agreement between atmospheric transport simulations of the release and the measured activity concentrations. Fig. 12 shows the simulated contribution from a release on 2023-10-20 15:00:00 UTC, lasting 1 h, compared with the measured results (as described in this paper). The forwards simulations are completed using HYSPLIT, with HRRR meteorological data (3 km spatial resolution), a 100 km^2 sampling grid and 24 h modelled from the simulated release. At this time the exact release magnitude is not known, however one of the key comparisons here is in the time axis, where the timing of the detection, based on the expected release time, is in good agreement since the contribution spills over two samples, which agrees with the measurement data, showing two consecutive detections of ^{127}Xe. Preliminary analysis of data collected from other fielded instruments is in agreement with the conclusion that ^{127}Xe was released from the tunnel around this time. The Q_B system provided a radionuclide detection at the farthest stand-off distance from the tunnel.

The activity concentration results are in close agreement with those calculated from another method, however the same GEANT4 simulation has underpinned the quantification (Eslinger et al., 2024). There are some key indications that the results are trustworthy. First of all, different ROIs have been used between the Xcounts and NCC method; secondly there is good agreement on the activity concentration calculated at each different ROI in the coincidence spectrum; and finally the results are underpinned by validation work which shows the measured activity concentrations are accurate when compared to a reference value (see Robinson et al., 2024 and Section 2.1).

The results from this analysis and others are useful to continue to develop and test atmospheric dispersion calculations associated with the experiment. The high level of quality control checks and careful validation of these results provide a trustworthy dataset which can now be used as part of multi-phenomenology data interpretations.

5. Conclusions

The SAUNA Q_B data from the PE1 experiment has been analysed and using a GEANT4 simulation and validation measurements, the activity concentrations of ^{127}Xe in each sample were calculated. There are two samples with detections of ^{127}Xe, the first is above the 95 % confidence limit (MDC), the second is above the 68 % confidence limit (L_c).

There is some agreement between the arrival time of a simulated release of radioxenon, which correlates with a known release event following turn-on of the P-Tunnel ventilation system. The data and analysis can be used to better understand the release magnitude and source term profile, and its relevance to low yield nuclear monitoring.

CRediT authorship contribution statement

M.A. Goodwin: Writing – review & editing, Writing – original draft, Software, Project administration, Methodology, Formal analysis, Data

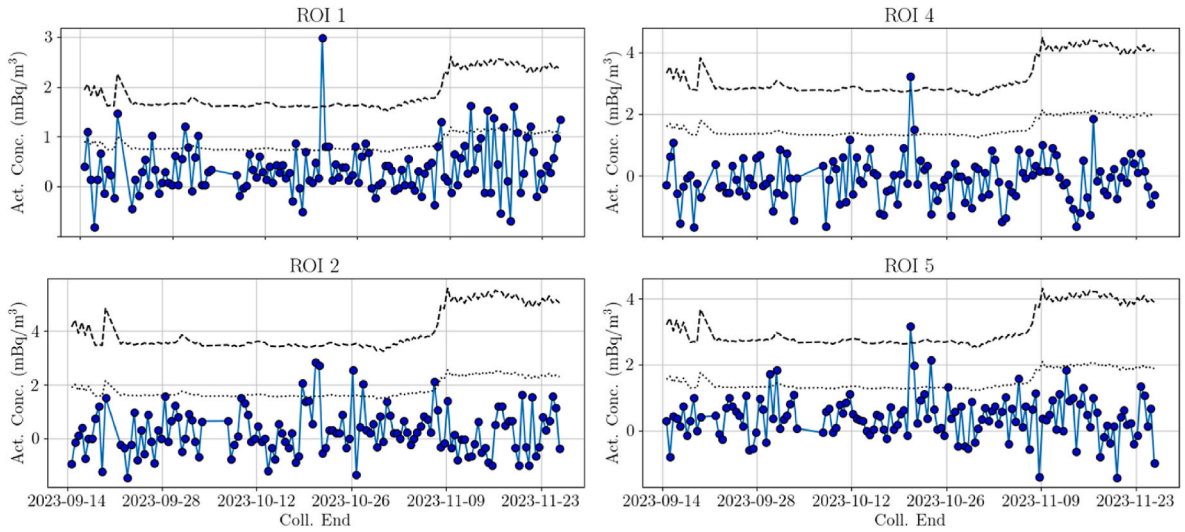

Fig. 10. Calculated activity concentrations of ^{127}Xe in ROIs 1,2,4,5 throughout the sampling period. Uncertainty bars are excluded for clarity of the plot and are approximately 7 % at k = 1. The dashed line represents the MDC and the dotted line represents the Lc.

Table 4
Activity concentration results for samples containing^{127}Xe above the critical limit (around 1.2 mBq/m^3). Alternative activity concentrations determined by (Eslinger et al., 2024).

Coll. Start (UTC)	Coll. End (UTC)	Xe. Vol (cm^3)	Act. Conc (mBq/m^3)	+/− (k = 1)	MDC (95 %)	Lc (68 %)	Act. Conc. (Eslinger et al., 2024) (mBq/m^3)
2023-10-20 04:38	2023-10-20 16:38	1.31	3.08	0.22	2.72	1.22	2.83
2023-10-20 16:38	2023-10-21 04:38	1.32	1.75	0.13	2.71	1.23	1.42

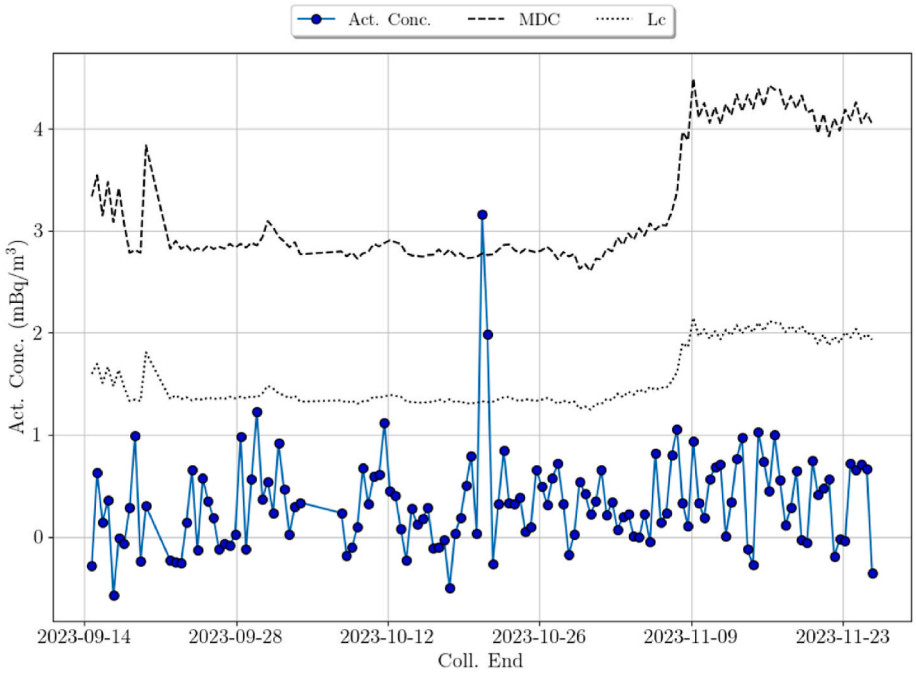

Fig. 11. Calculated ^{127}Xe activity concentrations and taking the mean of results in ROIs 1,2,4,5. The Lc and MDC are calculated as the mean results of respective Lc and MDC values for each ROI (1,2,4,5).

curation. **D.L. Chester:** Data curation. **G. Galvin:** Data curation. **P.W. Eslinger:** Writing – review & editing, Formal analysis. **M. Foxe:** Resources, Project administration, Funding acquisition, Data curation, Conceptualization. **J. Ely:** Writing – review & editing, Formal analysis. **R. Turley:** Resources, Data curation.

6. Disclaimer

The views expressed by the authors do not necessarily reflect those of AWE, PNNL or NNSS.

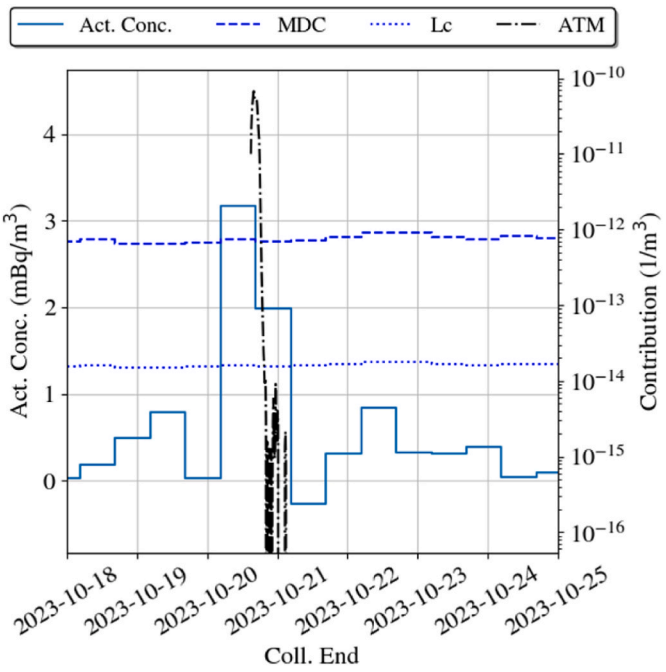

Fig. 12. Measured ^{127}Xe activity concentration time series, as determined in this work, plotted on the same x-axis as a simulated release of magnitude 1 unit, showing a contribution to the Q_B location around during the end of the first ^{127}Xe detection, and into the second ^{127}Xe detection.

Funding

The NNSS work was done by Mission Support and Test Services, LLC, under Contract No. DE-NA0003624 with the U.S. Department of Energy, and the National Nuclear Security Administration's Office of Defence Nuclear Non-proliferation. DOE/NV/03624–2006.

This Low Yield Nuclear Monitoring (LYNM) research was funded by the National Nuclear Security Administration, Defence Nuclear Non-proliferation Research and Development (NNSA DNN R&D). The authors acknowledge important interdisciplinary collaboration with scientists and engineers from LANL, LLNL, NNSS, PNNL, SNL and AWE in the UK. AWE work was funded by the UK Defence Nuclear Organisation, Nuclear Threat Reduction (UK MoD).

Declaration of competing interest

The authors declare that they have no known competing financial interests or personal relationships that could have appeared to influence the work reported in this paper.

Acknowledgements

The authors are indebted to Troy Robinson (INL) who provided AWE with samples of ^{127}Xe for measurement and analysis, which made the calibration checks possible. Further to the author list, the AWE team included several key people without whom the measurement campaign would not have been as successful. These include Claire Watt, Helen White, David Green, Ayrton Jenkins, Richard Cruttenden, Will Sparrow, Richard Hartnett and Ashley Davies.

Data availability

Data will be made available on request.

References

Bowyer, T.W., 2021. A review of global radioxenon background research and issues. Pure Appl. Geophys. 178 (2021), 2665–2675. https://doi.org/10.1007/s00024-020-02440-0.

Cagniant, A., Le Petit, G., Nadalut, B., Gross, P., Richard-Bressand, H., Fontaine, J.-P., Douysset, G., 2014. On the use of ^{127}Xe standards for the quality control of CTBTO noble gas stations and support laboratories. Appl. Radiat. Isot. 89, 176–185. https://doi.org/10.1016/j.apradiso.2014.02.003. ISSN 0969-8043.

Eslinger, P.W., Ely, J., Cooper, M.W., Foxe, M., Hayes, J.C., Mayer, M.F., Panisko, M.E., Sarathi, R., 2022. Determining the source of unusual xenon isotopes in samples. J. Environ. Radioact. 247, 106853. https://doi.org/10.1016/j.jenvrad.2022.106853.

Eslinger, P.W., Goodwin, M.A., Sarathi, R., et al., 2024. Detecting ^{127}Xe in an Atmospheric Tracer Experiment, Manuscript Submitted to Journal of Environmental Radioactivity.

Glueckauf, E., 1951. The Composition of Atmospheric Air. American Meteorological Society, Boston, MA, pp. 3–10. https://doi.org/10.1007/978-1-940033-70-9_1.

Goodwin, M.A., Britton, R., Davies, A.V., Bell, S.J., Collins, S.M., Regan, P.H., 2020. A high-resolution $\beta - \gamma$ coincidence spectrometry system for radioxenon measurements. Nucl. Instrum. Methods Phys. Res. A 978, 164452. https://doi.org/10.1016/j.nima.2020.164452.

Goodwin, M.A., Davies, A.V., Britton, R., Miley, H.S., Eslinger, P.W., Hoffman, I., Ungar, K., Mekarski, P., Botti, A., 2024a. Radionuclide measurements of the international monitoring system. J. Environ. Radioact. 272, 107357. https://doi.org/10.1016/j.jenvrad.2023.107357. ISSN 0265-931X.

Goodwin, M.A., Petts, A., Milbrath, B.D., et al., 2024b. Characterising the radionuclide fingerprint of an advanced gas-cooled nuclear power reactor. Pure Appl. Geophys. https://doi.org/10.1007/s00024-024-03488-y.

Hashizume, A., 2011. Nuclear data Sheets for A=127. Nucl. Data Sheets 112, 1647–1831.

Klingberg, F.J., Biegalski, S.R., Haas, D., Prinke, A., 2015. ^{127}Xe coincidence decay analysis in support of CTBT verification. J. Radioanal. Nucl. Chem. 305, 225–232. https://link.springer.com/article/10.1007/s10967-014-3871-x.

Miley, H.S., Eslinger, P.W., 2022. Impact of industrial nuclear emissions on nuclear explosion monitoring. J. Environ. Radioact. 257, 107081. https://doi.org/10.1016/j.jenvrad.2022.107081. ISSN 0265-931X.

Myers, S.M., et al., 2024. A multi-physics experiment for low-yield nuclear explosion monitoring. Technical Report. https://www.osti.gov/biblio/2345984.

Ringbom, A., Larson, T., Axelsson, A., Elmgren, K., Johansson, C., 2003. SAUNA—a system for automatic sampling, processing, and analysis of radioactive xenon. Nucl. Instrum. Methods Phys. Res., Sect. A 508 (3), 542–553. https://doi.org/10.1016/S0168-9002(03)01657-7. ISSN 0168-9002.

Ringbom, A., Fritioff, T., Aldener, M., Axelsson, A., Elmgren, K., Hellesen, C., Karlkvist, L., Kastlander, J., Olsson, H., Berglund, H., Hellman, B., Pettersson, O., 2023. SAUNA Q_B – array: the realization of a new concept in radioxenon detection. J. Environ. Radioact. 261, 107136. https://doi.org/10.1016/j.jenvrad.2023.107136.

Robinson, T., Goodwin, M.A., Foxe, M., et al., 2024. ^{127}Xe Quantification Method Development and Intercomparison Exercise, Manuscript Submitted to Applied Radiation & Isotopes.

United Nations, 1996. The comprehensive nuclear-test-ban treaty. Number Resolution CTBT/MSS/RES/1. United Nations.